



**HAL**  
open science

## Characterization of transport of titanium neutral atoms sputtered in Ar and Ar/N 2 HIPIMS discharges

A El Farsy, J. Ledig, M Desecures, J. Bougdira, L. de Poucques

► **To cite this version:**

A El Farsy, J. Ledig, M Desecures, J. Bougdira, L. de Poucques. Characterization of transport of titanium neutral atoms sputtered in Ar and Ar/N 2 HIPIMS discharges. *Plasma Sources Science and Technology*, 2019, 28 (3), pp.035005. 10.1088/1361-6595/ab022b . hal-02319596

**HAL Id: hal-02319596**

**<https://hal.science/hal-02319596>**

Submitted on 18 Oct 2019

**HAL** is a multi-disciplinary open access archive for the deposit and dissemination of scientific research documents, whether they are published or not. The documents may come from teaching and research institutions in France or abroad, or from public or private research centers.

L'archive ouverte pluridisciplinaire **HAL**, est destinée au dépôt et à la diffusion de documents scientifiques de niveau recherche, publiés ou non, émanant des établissements d'enseignement et de recherche français ou étrangers, des laboratoires publics ou privés.

# 1 Characterization of transport of Titanium neutral atoms 2 sputtered in **Ar and Ar/N<sub>2</sub>** HIPIMS discharges 3

4 A el Farsy<sup>1, \*</sup>, J Ledig<sup>1</sup>, M Desecures<sup>1</sup>, J Bougdira<sup>1</sup>, L de Poucques<sup>1</sup>  
5

6 <sup>1</sup> Institut Jean Lamour UMR 7198, CNRS - Université de Lorraine, Campus ARTEM, F-  
7 54011 Nancy, France.  
8

9 \* Corresponding author: [abderzak.el-farsy@univ-lorraine.fr](mailto:abderzak.el-farsy@univ-lorraine.fr)

## 10 Abstract

11 We report in this work the investigation of the transport behavior of Ti neutral atoms  
12 sputtered in reactive high power impulse magnetron sputtering (R-HiPIMS) device  
13 used for TiN coating deposition. The time resolved tunable diode laser induced  
14 fluorescence (TR-TDLIF), previously developed to study the transport of tungsten  
15 atoms, was improved to measure Ti neutral atoms velocity distribution functions. We  
16 find that the TR-TDLIF signal has to be fitted using three Gaussian distributions,  
17 corresponding to the energetic (EN), thermalized (TH) and quasi-thermalized (QTH:  
18 TH atoms with non-zero mean velocity) atoms populations. Then, the ability to  
19 distinguish populations of atoms and to determine their corresponding deposited flux  
20 and energy may be of great interest to control film properties as desired for targeted  
21 applications. From the fitting, the vapor transport parameters (flux and energy) are  
22 calculated and studied as function of distance from the target, pressure and percentage  
23 of nitrogen in Ar/N<sub>2</sub> gas mixture. The study focuses on the effect of added nitrogen on  
24 the transport of sputtered atoms.

25 **Keywords:** time resolved tunable diode laser induced fluorescence, reactive  
26 magnetron sputtering, high power impulse magnetron sputtering (HiPIMS), atoms  
27 velocity distribution function, transport of sputtered atoms, titanium, nitrogen

## 28 I. Introduction

29 Since the 1970s, magnetron sputtering (MS) process has been developed for the growth of  
30 thin films by physical vapor deposition (PVD) [1]. The developments of conventional reactive  
31 direct current (R-dcMS) and radiofrequency (R-rfMS) magnetron sputtering methods allow  
32 the deposition of a wide range of thin films of materials such as metals, oxides, nitrides,  
33 ceramics, etc. [2]. Consequently, MS is a widely used deposition technology in many  
34 industrial applications.

35        **In conventional magnetron sputtering discharges**, sputtered species are mainly emitted by  
36 the cathode as neutral particles and ions of the sputtered material do not contribute  
37 significantly to the deposition process. Ionized Physical Vapor Deposition (IPVD) reactors  
38 have then been developed since the 1990s to improve the quality of deposited films in terms  
39 of mechanical properties (higher density, reduced porosity, better resistance to corrosion) and  
40 of conformity for deposition on complex substrate geometry [3-8]. The main goal of IPVD is  
41 to ionize a fraction of neutral species sputtered from the magnetron target in order to transfer  
42 potential energy to ions, and to collimate and control the obtained ion particle fluxes by  
43 applying a negative bias voltage to the substrate. IPVD reactors consist of a magnetron  
44 discharge assisted by an additional plasma source, located in the area between the substrate  
45 and the magnetron cathode, which ionizes the sputtered vapor flowing from the magnetron.  
46 Reactors using helicon [9], electron cyclotron resonance (ECR) coupled discharge [10] or  
47 microwave surface wave plasma [11] have been studied but most of the IPVD reactors used  
48 radio-frequency coils (RF-IPVD) to create the additional ionization [4, 5, 12, 13]. Some  
49 difficulties, however, have to be tackled in RF-IPVD processes. Indeed, the necessary  
50 modifications of the reactor chamber design and the fact that the internal antenna immersed in  
51 the reactor could pollute the deposition process [13-15], present potential inconveniences for  
52 some applications. Moreover, the ionization degree may be too low for specific applications  
53 such as the filling of trenches, as well as for new functional coatings demands.

54        Therefore, high power impulse magnetron sputtering process (HiPIMS) has been  
55 developed [16] and intensively studied since the end of the 1990s [17-22], and reactive  
56 HiPIMS (R-HiPIMS) has emerged since 2002 [23] for the adhesion enhancement of CrN hard  
57 coatings on steel [24]. In HiPIMS process, the high power (a few kW.cm<sup>-2</sup>) is turned on  
58 during short pulses (tens of μs) in order to avoid the cathode overheating and arc formation.  
59 The plasma density is usually between 10<sup>12</sup> and 10<sup>13</sup> cm<sup>-3</sup> [16, 25] and the ionization degree of  
60 the sputtered particles is greater than 50 % [25]. The main advantage of HiPIMS and R-  
61 HiPIMS technologies is the absence of an additional ionization antenna in the reactor  
62 chamber, i.e. an industrial reactor can be upgraded to a HiPIMS one only by changing the  
63 power supply. Furthermore, in R-HiPIMS process, the poisoning of the target and the plasma  
64 composition are not only induced by the partial pressure of the reactive gas and the power as  
65 in dcMS, since discharge duration and pulse repetition rates are also key parameters for the  
66 balance between sputtering and sticking of reactive species [26].

67        For a better understanding of both non-reactive and reactive HiPIMS discharges, the  
68 development of time and/or space resolved suitable diagnostics allowing the study of neutral  
69 and ionic particle fluxes (densities and energies) between the target and the substrate is  
70 required. The objectives are to control and optimize the deposition process. Ion energy  
71 distribution functions (IEDFs) of ions created from the ionization of sputtered particles and  
72 the gas are often measured by time-average and/or time-resolved mass spectrometry [27-32].  
73 Moreover, some measurements of charged and neutral (since a significant fraction of neutral  
74 species remains and may influence thin film deposition properties) particles were carried out  
75 by time-resolved and space-resolved optical emission spectroscopy [33, 34], laser induced

76 fluorescence with a YAG:Nd laser [35] or resonant optical absorption spectroscopy [36].  
77 Recently, the velocity distribution of sputtered titanium in the target vicinity of a HiPIMS  
78 discharge, and the relaxation from Thompson distribution to Maxwell one, were reported by  
79 Held *et al.* [37].

80 In previous papers [38, 39], we presented new measurements of atoms velocity  
81 distribution functions (AVDFs) of the metastable state of neutral tungsten (W) obtained by  
82 means of time resolved tunable diode laser induced fluorescence (TR-TDLIF) in non-reactive  
83 (pure Ar gas) HiPIMS discharges. The present work is focused on R-HiPIMS process study  
84 used for titanium nitride (TiN) thin film deposition. TiN was chosen for its good mechanical  
85 and optical properties, excellent chemical resistance and good biocompatibility. However, the  
86 scope of this paper is not devoted to film properties. Thin films were deposited in order to  
87 compare and corroborate TR-TDLIF measurements and deposition rate (estimated by  
88 scanning electron microscopy). The main goal is to develop TR-TDLIF on the ground state of  
89 neutral Ti atoms. Indeed, this method performed on W has been drastically improved to be  
90 able to measure the very low intensity of the Ti fluorescence signal, especially when N<sub>2</sub> is  
91 added in the Ar/N<sub>2</sub> gas mixture (owing to the high decrease of number of Ti atoms sputtered  
92 from the poisoned target). Furthermore, the appearance, reduction or vanishing of hysteresis  
93 [see 26 and therein] is not discussed here because the main objective is to present reliable TR-  
94 TDLIF measurements. We report the evolution of Ti AVDFs showing the different stages of  
95 the atoms transport and highlighting an intermediate regime between ballistic and diffusive  
96 ones (named quasi-diffusive or quasi-thermalized). Spatio-temporal evolutions of absolute  
97 densities, fluxes and energies are characterized by varying the percentage of N<sub>2</sub> in the gas  
98 mixture. This study may be a significant step in the ability to control film properties.

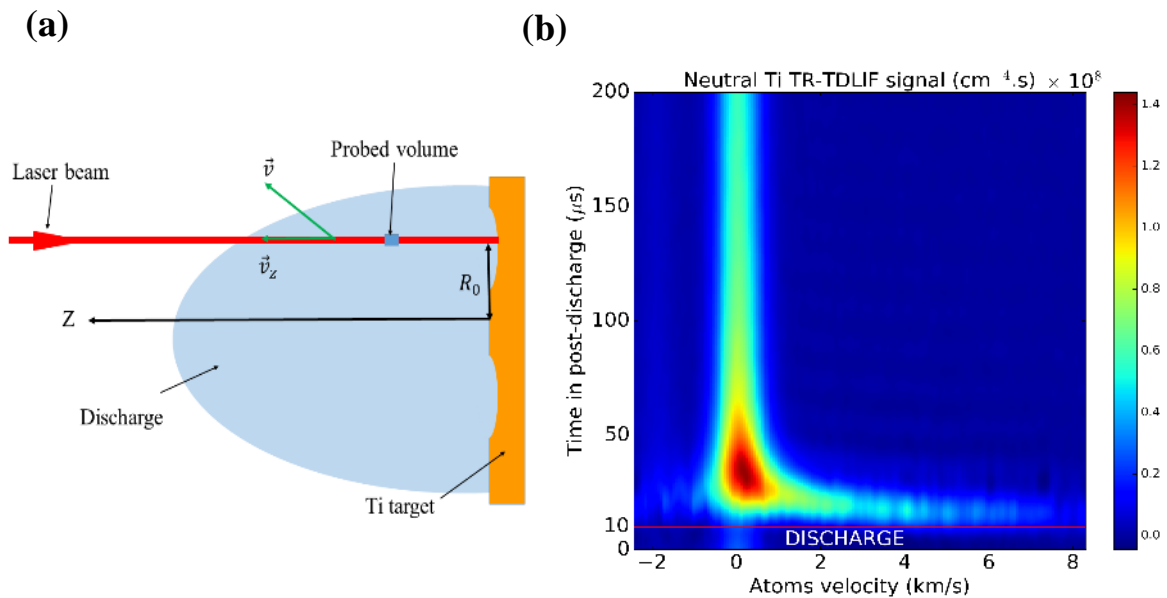
## 99 II. Experimental setup

100 As presented in a previous work [40] our reactor was used to develop the time resolved  
101 tunable diode laser induced fluorescence measurements. The **balanced** magnetron cathode is  
102 fitted with a water cooled Titanium target of 5 cm in diameter, 3 mm in thickness and 99.99%  
103 of purity. Prior to discharge process, the vacuum reaches a pressure lower than  $2 \times 10^{-4}$  Pa. Ar  
104 and N<sub>2</sub> gases were added into the chamber with various N<sub>2</sub>/Ar flow rate ratio (0-10%) while  
105 the total flow rate was fixed at 18 sccm. The TR-TDLIF measurements were carried out at  
106 fixed discharge power ( $350 \text{ W.cm}^{-2}$ ) and discharge time ( $T_d=10 \text{ } \mu\text{s}$  and  $f=1 \text{ kHz}$ :  
107 corresponding to a duty cycle of 1%). These parameters have an important role in the  
108 process. **Indeed, we have not studied the repetition frequency and the pulse duration, but**  
109 **Magnus *et al.* [41] reported that the repetition frequency has an effect on the transition from**  
110 **metallic to compound mode. In addition, Ferrec *et al.* [28] reported that at small average**  
111 **HiPIMS power ( $7 \text{ W cm}^{-2}$ ) a long discharge time produces more argon ions whereas a short**  
112 **one generates more metallic ions whereas Konstantinidis *et al.* [42] suggested the reverse at**  
113 **higher power due to the sputtering wind (inducing a local decrease of the argon density,**  
114 **consequently Ar ions density, due to the intense target sputtering gas rarefaction). In fact,**  
115 **these parameters, especially the short  $T_d$  and the limited HiPIMS power, were mainly chosen**  
116 **to separate the discharge from the post-discharge and to perform TR-TDLIF measurement**  
117 **close to the target surface (at  $z=1.3 \text{ cm}$  since the sputtered Ti get thermalized quickly by**

118 collisions with the background gas) and study the transport of metallic vapor with limited  
 119 disturbances linked to the plasma (strong optical emission at high power discharge and Ti  
 120 atoms production during a long time when using a long  $T_d$ ).

121 Diode laser (DL) used to excite the neutral sputtered atoms, Toptica Phototonics DL 100 (20  
 122 mW), provide a 14 pm wavelength range ( $\lambda_{\text{laser}}$ ) without mode hop and centered at  $\lambda_0=398.170$   
 123 nm (the same transition used by Sushkov *et al.* [43]), which is suitable to probe wide range of  
 124 sputtered atoms velocities. The DL has a high spectral resolution (0.005 pm) compared to that  
 125 of an OPO laser ( $\sim 2$  pm) or a dye Nd:YAG laser ( $\sim 0.5$  pm).  $\lambda_0$  corresponds to the neutral Ti  
 126 resonance transition from the ground state level  $3d^24s^2 - (a^3F_2)$  to the short lifetime radiative  
 127 excited level  $3d^2(^3F)4s4p(^1P^o) - (y^3F_2)$ . The fluorescence signal ( $\lambda_{\text{LIF}}$ ) also emitted at  $\lambda_{\text{laser}}$ .  
 128 The detailed description of the optical and electrical arrangements can be found in a previous  
 129 work [38]. The HiPIMS unit was set to deliver 180 pulses during the 14-pm wavelength scan.  
 130 The wavelength variation during one HiPIMS pulse period (1 ms) is assumed to be negligible  
 131 since it generates a Doppler shift error of 0.077 pm. This corresponds to a 60 m/s error on  
 132 velocity while the measured velocities are in the order of km/s. The laser beam probes the  
 133 axial (perpendicular to the target surface) velocity component of sputtered atoms ( $\vec{v}_z$ , see  
 134 figure 1 (a)). The magnetron target was moved in z direction ( $z=0$  cm corresponding to the  
 135 target surface) to perform measurements at various “target/probed volume” distances. **All**  
 136 **measurements were carried out between  $z=1.3$  cm and 8 cm above the racetrack and at  $R_0=1.3$**   
 137 **cm from the center of the target. At  $z=1.3$  cm, the B value is lower than 20G and quasi-**  
 138 **homogeneous.**

139



140 **Figure 1:** (a) Experimental set-up for TR-TDLIF measurements of sputtered Ti atoms in the axial  
 141 direction (perpendicular to the target surface). (b) Typical Ti neutral sputtered atoms distribution  
 142 measured at  $z=1.3$  cm,  $R_0=1.3$  cm,  $p=0.7$  Pa,  $P= 350\text{W.cm}^{-2}$ , and with pure Argon gas.

143 In order to obtain absolute measurements, time resolved tunable diode laser absorption  
144 spectroscopy (TR-TDLAS) was used to calibrate the TR-TDLIF signal. The absorption  
145 process has to be as homogeneous as possible along the laser beam path (absorption length)  
146 during TR-TDLAS measurement. Thus, the calibration was performed in conditions where  
147 the sputtered atoms have isotropic distribution (thermalized vapor), *i.e.* far away from target  
148 ( $z=8$  cm), at relatively high pressure ( $p=2.7$  Pa) and at the end of the post-discharge (700-  
149 900 $\mu$ s). The contributions of the Stark and pressure broadenings were neglected due to the  
150 low electron density/electric field in the post-discharge and the very low working gas pressure  
151 (between 0.7 and 2.7 Pa). Furthermore, Zeeman effect does not contribute to line broadening  
152 in our conditions. Only Doppler broadening and shift are, then, taking into account.  
153 Therefore, to convert the laser wavelength scale ( $\Delta\lambda_{\text{laser}} = \lambda_{\text{laser}} - \lambda_0$  was determined by means  
154 of a Fabry-Pérot interferometer) into the velocity scale, the classical Doppler's relation  
155 ( $v=c\cdot\Delta\lambda_{\text{laser}}/\lambda_0$ ) was applied. Figure 1 (b) shows a typical 2D-image of the AVDF (atoms  
156 velocity  $v_z$ ,  $t$ ) of the Ti neutral atoms velocity distribution functions measured with TR-  
157 TDLIF in a HiPIMS post-discharge.

### 158 **III. Results and discussions**

#### 159 **III-1. Quasi-thermalized atoms with non-zero mean velocity**

160 Time resolved tunable diode laser induced fluorescence measurements give access to the  
161 atoms velocity distribution functions (AVDF). The latter have to be theoretically fitted to  
162 distinguish the various atoms populations and to calculate their related properties: density,  
163 flux, energy, etc.

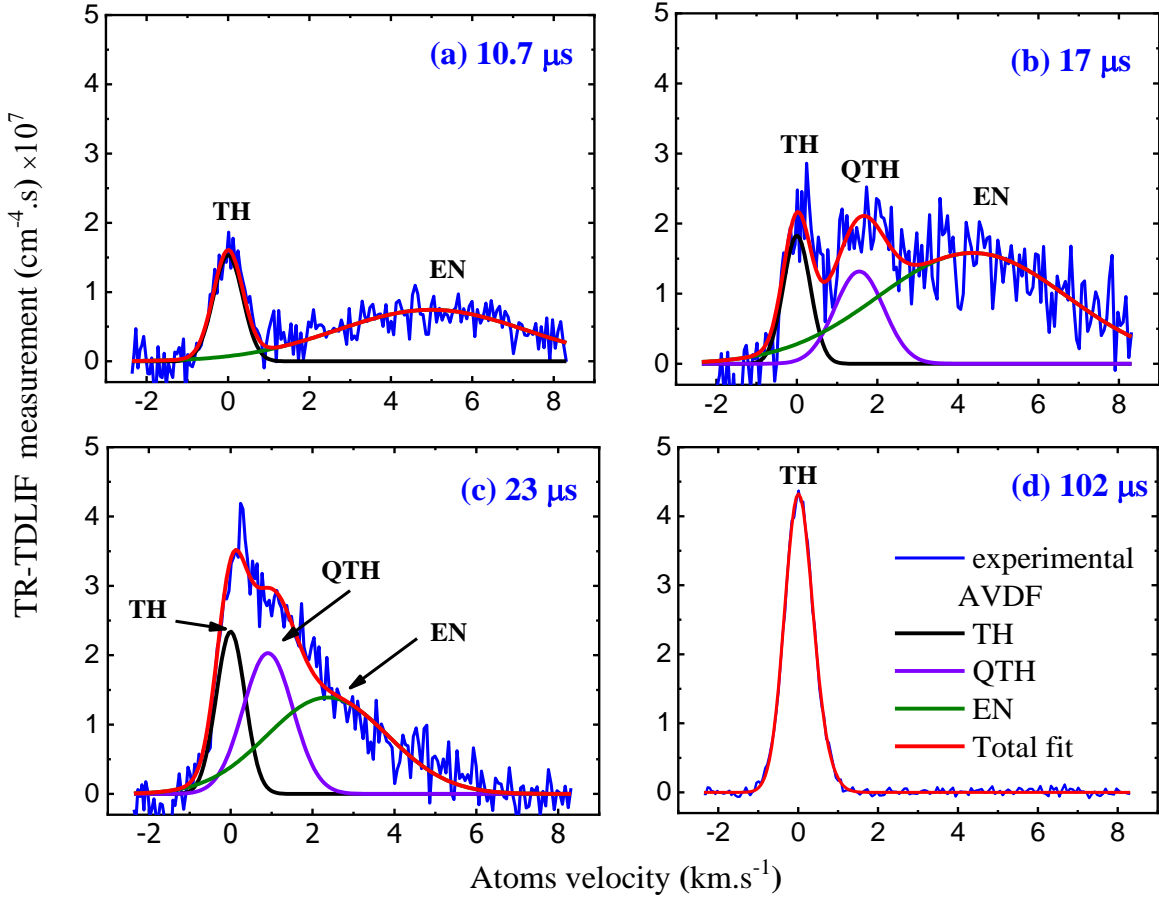
164 In a previous work, Desecures *et al.* [39] studied the transport of tungsten sputtered atoms in  
165 HiPIMS discharge and showed that two populations coexist: the anisotropic and thermalized  
166 atoms. Then, the TR-TDLIF signal has been fitted using two Gaussian distributions.  
167 However, after carrying an extensive analysis of the parameters evolutions in the post-  
168 discharge, we have concluded that the anisotropic population contains itself two populations:  
169 the energetic atoms and quasi-thermalized atoms with non-zero mean velocity. The different  
170 stages of atoms transport were then accessible. When Ti atoms collide with Ar atoms, they  
171 lose in average 50% of their initial energy, contrary to W atoms which lose only 30% (see  
172 table 1). In fact, a sputtered Ti atom with energy of 4 eV (average energy of Ti EN atoms  
173 ejected from the target is, depending on the cathode voltage, usually between 3 and 5 eV)  
174 becomes thermalized after 7-8 collisions but the thermalization of a sputtered W atom with  
175 same energy needs 11-12 collisions.

176  
177  
178  
179

180 **Table 1:** Average fraction of energy lost ( $1 - E_f/E_i$ ) of the sputtered atoms after one  
 181 collision with the buffer gas ( $E_i$ =initial energy;  $E_f$ =final energy).

Sputtered atoms \ Gas		Ar (40 amu)	N <sub>2</sub> (28 amu)	N (14 amu)
W (183 amu)		0.30	0.24	0.14
Ti (48 amu)		0.50	0.47	0.35

182



183

184 **Figure 2 :** Neutral Titanium atoms velocity distribution functions measured with TR-TDLIF technique  
 185 at  $p = 2.7 \text{ Pa}$ ,  $z = 2 \text{ cm}$ ,  $P = 350 \text{ W.cm}^{-2}$  and pure Ar, for various times in the post-discharge : (a)  $10.7$   
 186  $\mu\text{s}$ , (b)  $17 \mu\text{s}$ , (c)  $23 \mu\text{s}$  and (d)  $102 \mu\text{s}$ .

187 It is important to point out that W atoms keep their momentum (direction and velocity) longer  
 188 due to their large mass compared with the buffer gas atoms, while Ti atoms evolve more  
 189 rapidly towards an isotropic distribution. To study the transport of Ti neutral sputtered atoms,  
 190 velocity distribution functions for different times in post-discharge are given in figure 2.  
 191 Figure 2(a) represents the AVDF at the beginning of the post-discharge ( $t = 10.7 \mu\text{s}$ ) and  
 192 clearly shows two populations (EN and TH). Indeed, one can observe that the experiment  
 193 curve is well fitted with two Gaussians. The population centered at  $v_z = 0$  corresponds to the  
 194 residual thermalized neutral atoms (TH) measured in the probed volume at the end of the

195 post-discharge (they cannot be new thermalized atoms produced during  $t=10.7 \mu\text{s}$  from the  
 196 beginning of the short discharge time -  $T_d=10 \mu\text{s}$ ). The second population centered at  $v_z=4.5$   
 197  $\text{km.s}^{-1}$  represents the new high velocity sputtered atoms created during the discharge (EN  
 198 distribution function). Figures 2(b) and 2(c) highlight unexpected profiles at intermediate  
 199 times ( $t=17$  and  $23 \mu\text{s}$ ). They clearly show a third peak at  $v_z=1.5 \text{ km.s}^{-1}$  for  $t=17 \mu\text{s}$  and  $1$   
 200  $\text{km.s}^{-1}$  for  $t=23 \mu\text{s}$ . Since the fit with two Gaussians, we have assumed that AVDF is the sum  
 201 of three populations. This third population is an intermediate population between EN (ballistic  
 202 transport) and TH (diffusive transport) ones. Its average energy is  $\sim 0.5 \text{ eV}$  at  $t=17 \mu\text{s}$ ,  $\sim 0.2 \text{ eV}$   
 203 at  $t=23 \mu\text{s}$ , and decreases down to the thermal energy of TH atoms ( $\sim 0.05 \text{ eV}$ ) for later times  
 204 in the post-discharge. That is the reason this population is named ‘‘QTH: Quasi Thermalized  
 205 Atoms’’, for TH atoms with a non-zero mean velocity. It is produced by collisions of EN  
 206 atoms with the buffer gas and a few collisions are missing to reach a complete isotropic  
 207 AVDF (mean velocity=zero). In figure 2(d) one can notice that only one Gaussian (TH  
 208 population) is needed to well fit the experimental TR-TDLIF signal at  $t=102 \mu\text{s}$  because EN  
 209 atoms have already crossed the probed volume ( $z=2 \text{ cm}$ ) at this late time in the post-  
 210 discharge.

### 211 III-2. Time evolution of sputtered atoms properties in the post- 212 discharge

213 From the fit of the TR-TDLIF measurements with three Gaussians, time evolutions of TH,  
 214 QTH and EN populations are determined. The integrals over  $v_z$  ( $v_z>0$  in order to take into  
 215 account only atoms going towards the probed volume or substrate) of the AVDF for each TH,  
 216 EN and QTH population, at any time in the post-discharge, define the densities of neutral  
 217 atoms  $[\text{Ti}]_{\text{TH}}(t)$ ,  $[\text{Ti}]_{\text{EN}}(t)$  and  $[\text{Ti}]_{\text{QTH}}(t)$ :

$$218 \quad [\text{Ti}]_i(t) = \int_0^\infty \text{AVDF}_i(v_z, t) dv_z \quad (1)$$

219 where  $i = \text{TH, EN or QTH}$ .

220 Similarly, the integrals of  $\text{AVDF} \times v_z$  give the fluxes directed (deposited fluxes) towards the  
 221 substrate  $\Phi_{\text{TH}}(t)$ ,  $\Phi_{\text{EN}}(t)$  and  $\Phi_{\text{QTH}}(t)$ :

$$222 \quad \Phi_i(t) = \int_0^\infty v_z \text{AVDF}_i(v_z, t) dv_z \quad (2)$$

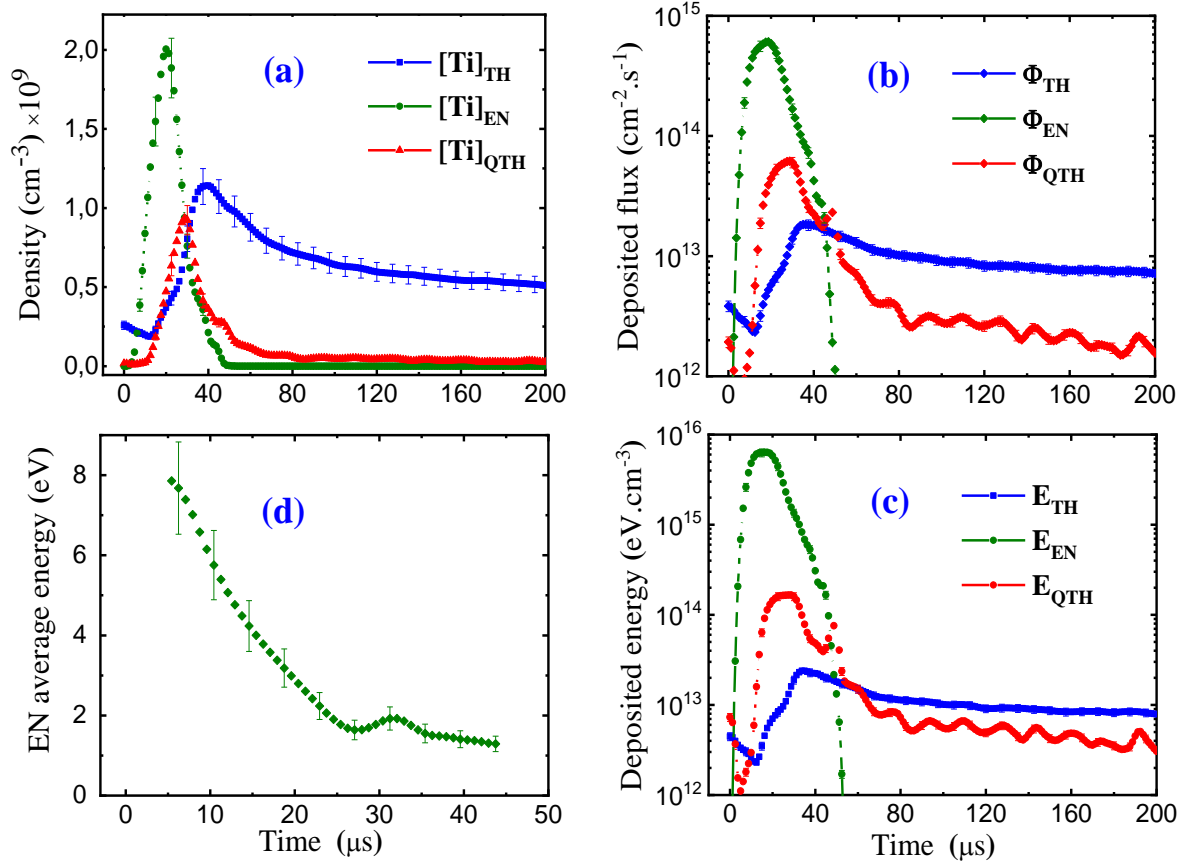
223 The integrals of  $\text{AVDF} \times v_z^2 \times m/2$  give deposited energies  $E_{\text{TH}}(t)$ ,  $E_{\text{EN}}(t)$  and  $E_{\text{QTH}}(t)$ :

$$224 \quad E_i(t) = \frac{1}{2} m \int_0^\infty v_z^2 \text{AVDF}_i(v_z, t) dv_z \quad (3)$$

225 The average energy of each population atoms is defined as:

$$226 \quad E_{\text{Av-i}}(t) = \frac{E_i(t)}{\int_0^\infty \text{AVDF}_i(v_z, t) dv_z} \quad (4)$$

227  
 228



229 **Figure 3:** Temporal variations of density (a), deposited flux (b) and deposited energy (c) of  
 230 thermalized (TH), energetic (EN) and quasi-thermalized (QTH) atoms populations. Time evolution of  
 231 EN atoms average energy (d). At  $p=2.7$  Pa,  $z = 1.3$  cm,  $P=350$  W.cm<sup>-2</sup> and pure Ar.  
 232

233 Figure 3(a) shows the time evolutions of titanium ground state atoms densities at a distance  
 234 close to the target ( $z=1.3$  cm), at 2.7 Pa (pure Ar) and a HiPIMS power of 350 W.cm<sup>-2</sup>. As  
 235 shown in figure 3(d), the EN average energy ( $E_{av-EN}$ ) decreases in post-discharge from 8 eV to  
 236 1.5 eV. This high energy permits EN atoms to cross the probed volume in the first 50  $\mu$ s  
 237 (ballistic transport). As TH atoms have a much lower average energy ( $E_{av-TH} \sim 0.05$  eV) and a  
 238 diffusive regime of transport, they can be measured in the probed volume during the whole  
 239 post-discharge (1 ms). One can observe two slopes during the increase of  $[Ti]_{TH}(t)$ . The first  
 240 one occurs during the  $[Ti]_{QTH}(t)$  increase and the greater one during the  $[Ti]_{QTH}(t)$  drop. The  
 241 first slope seems to correspond to source term of TH atoms (by collisions of QTH atoms with  
 242 the buffer gas) with relatively low  $[Ti]_{QTH}$  (and  $E_{av-QTH}$  between 0.5 and 0.2 eV) and the  
 243 second one to higher source term with higher  $[Ti]_{QTH}$  (and  $E_{av-QTH}$  between 0.2 and 0.05 eV).  
 244 The drop of  $[Ti]_{QTH}(t)$  can be the result of the losses of QTH atoms, close to the target, which  
 245 are no more compensated by the term source of  $[Ti]_{QTH}$  (collisions of EN atoms with the  
 246 buffer gas). The time evolutions of the corresponding deposited flux and deposited energy are  
 247 plotted in figures 3(b) and 3(c). Unlike densities of the three populations, the deposited flux  
 248 maximum of EN atoms is at least ten times higher than the QTH and TH ones because the  
 249 mean velocity of EN population is much higher than the QTH and TH ones ( $\langle v \rangle_{EN} \gg \langle v \rangle_{QTH} \geq$   
 250  $\langle v \rangle_{TH}$ ). It is then more suitable to analyze the fluxes rather than densities to study the atoms  
 251 transport.

252 From curves of figures 3(b) and 3(c), the energy ( $E_i^{int}$ ) integrated over a HiPIMS period are  
 253 given by the following integral:

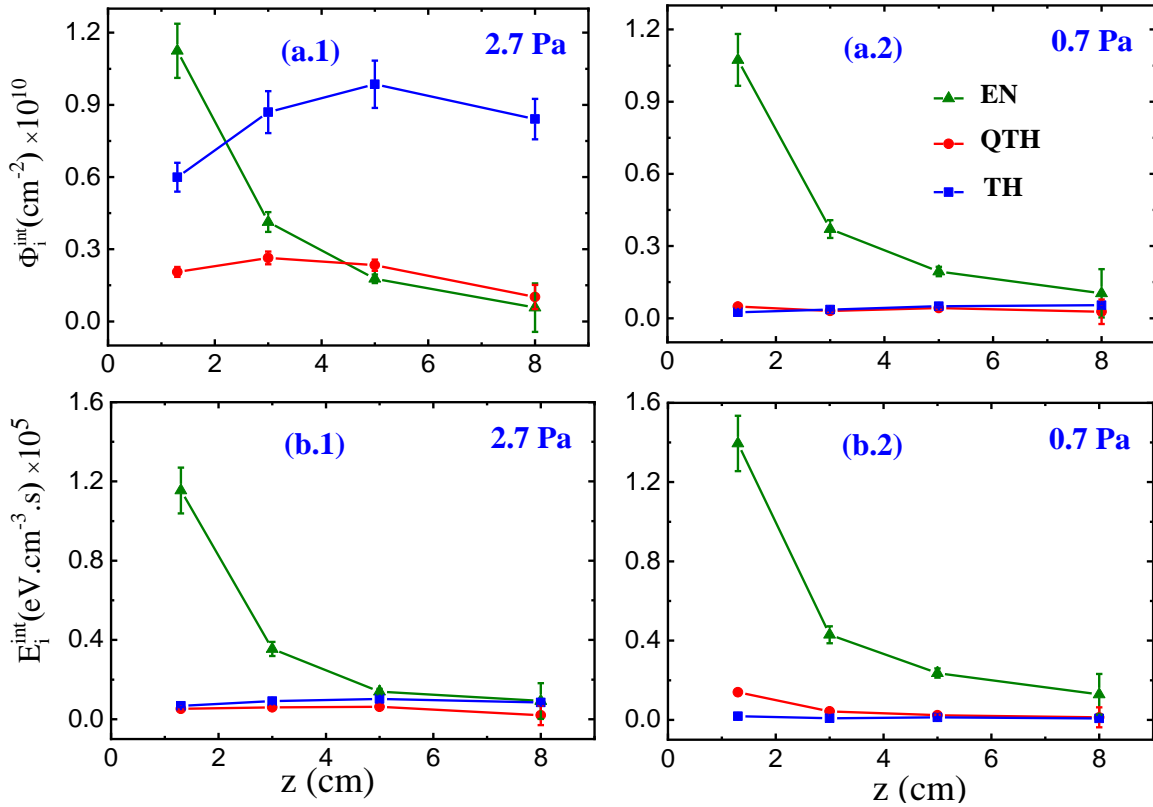
$$254 E_i^{int} = \int_0^{1ms} E_i(t) dt \quad (5)$$

255 where  $i = TH, EN$  or  $QTH$ .

256 The deposited flux ( $\Phi_i^{int}$ ) integrated over a HiPIMS period is defined as:

$$257 \Phi_i^{int} = \int_0^{1ms} \Phi_i(t) dt \quad (6)$$

258 This procedure was applied on TR-TDLIF measurements performed at two working pressures  
 259 ( $p=0.7$  and  $2.7$  Pa), HiPIMS average power of  $350W.cm^{-2}$  and as a function of the distance  
 260 from the target “z” (figure 4).

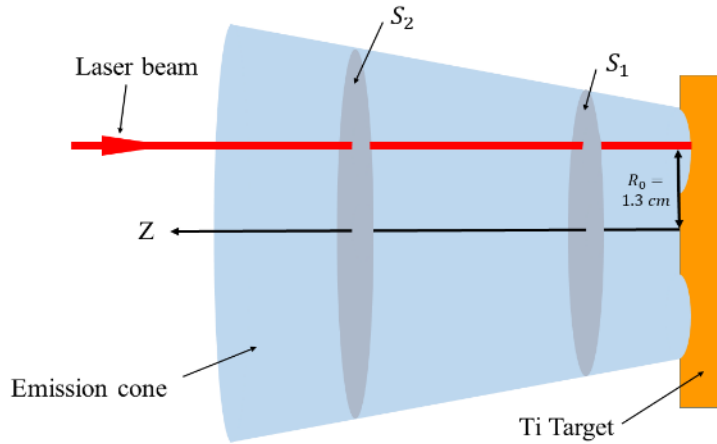


261

262 **Figure 4:** Axial evolutions of deposited fluxes ( $\Phi_{EN}^{int}$ ,  $\Phi_{QTH}^{int}$ ,  $\Phi_{TH}^{int}$ ) (a.1, a.2) and deposited  
 263 energies ( $E_{EN}^{int}$ ,  $E_{QTH}^{int}$ ,  $E_{TH}^{int}$ ) (b.1, b.2) at  $p= 2.7$  and  $p= 0.7$  Pa.  $R_0=1.3$  cm,  $P=350W.cm^{-2}$ ,  
 264 pure Ar.

265 At low pressure ( $0.7$  Pa) the EN deposited flux and energy are dominant, even at  $z=8$  cm  
 266 (figures 4(a.2) and 4(b.2)). As expected, increasing the pressure up to  $p=2.7$  Pa, sputtered  
 267 atoms undergoing more collisions, the TH atoms source term increases and their diffusive  
 268 transport becomes slower (inducing fewer TH atoms losses during one post-discharge in the  
 269 probed volume). Therefore, the main deposited flux depends on the distance from the target  
 270 (figure 4(a.1)) and the TH one becomes dominant for  $z>2$  cm in our conditions. However, due  
 271 to their high energy, the EN deposited energy remains the highest up to  $z\sim 8$  cm (figure  
 272 4(b.1)). In addition,  $\Phi_{EN}^{int}$  ( $0.7$  Pa) and  $\Phi_{EN}^{int}$  ( $2.7$  Pa) have the same behavior and nearly the

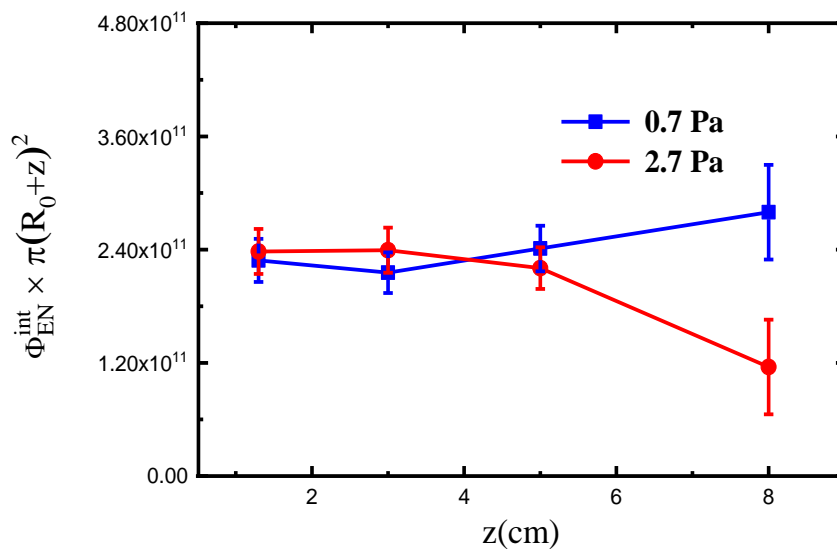
273 same values (except for  $z \sim 8$  cm). It means that EN atoms flux depends little on the pressure in  
 274 these ranges of parameters ( $p$  and  $z \leq 5$  cm). In fact, for these typical HiPIMS process  
 275 conditions, the effect of collisions seems then limited, *i.e.* only a few percent of EN atoms  
 276 produced during “one” of HiPIMS discharges are thermalized. TH flux shown in figure 4(a.1)  
 277 is probably the result of an accumulation of residual atoms on successive HiPIMS discharges.



278  
 279

*Figure 5: Scheme of the sputtered emission cone.*

280 For both pressures, the  $\Phi_{EN}^{int}(z)$  drop is mainly due to the emission cone of the sputtered atoms  
 281 (figure 5). Indeed, EN atoms are ejected in a cosine emission ejected distribution [3] (see  
 282 chapter 2, page 37), and consequently about 70% of the sputtered vapor is globally emitted in  
 283 a  $\theta = 45^\circ$  emission cone with respect to the normal of the target surface. In order to illustrate  
 284 this effect, we have assumed that the area of the emission cone section is given by  
 285  $S(z) \approx \pi(z+1.3)^2$ .



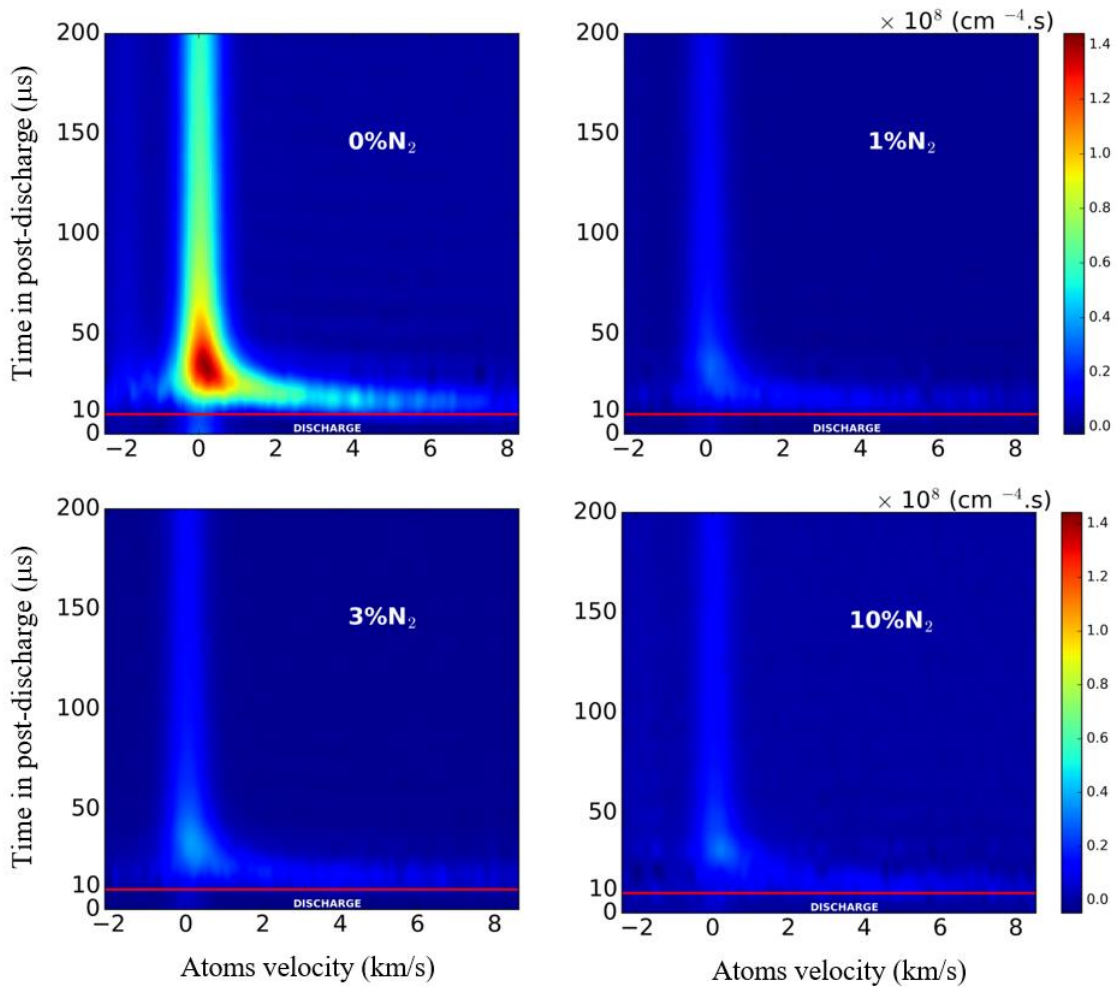
286  
 287

*Figure 6: Corrected deposited fluxes :  $\Phi_{EN}^{int} \times \pi(z+1.3)^2$ .*

288 The corrected deposited fluxes taking into account the cone section, *i.e.*  $\Phi_{EN}^{int} \times S(z)$  are plotted  
 289 in figure 6. At  $p=0.7$  Pa, the results show that the variations of the corrected deposited fluxes  
 290 are very small. The slight discrepancy observed at  $z=8$  cm is related to the weak measured  
 291 TR-TDLIF signal and the uncertainties of the fit (traduced by greater error bars in the figure).  
 292 Therefore, we can conclude that the losses of EN atoms during their transport towards the  
 293 probed volumes are mainly due to the dispersion in the sputtering emission cone. At higher  
 294 pressure (2.7 Pa), the real effect of collisions on EN atoms losses cannot be clearly  
 295 distinguished in the range  $0 \leq z \leq 5$  cm.

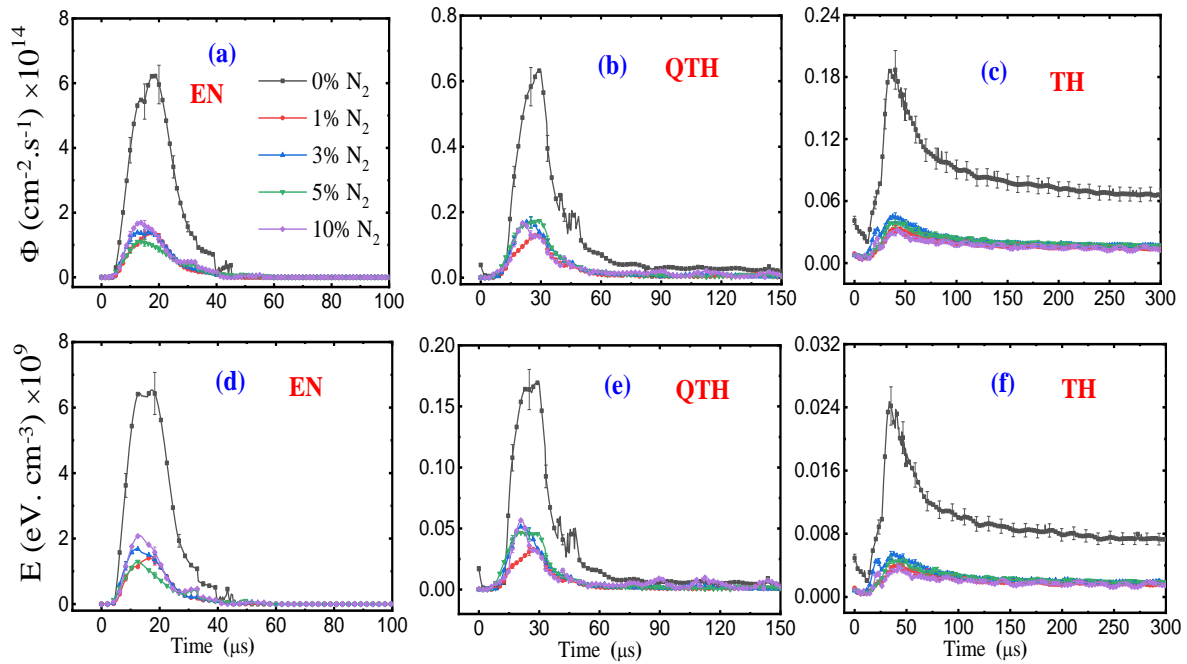
### 296 III-3. Characterization of the R-HiPIMS discharge (Ar/N<sub>2</sub>)

297 The above TR-TDLIF results give a comprehensive knowledge about the transport of the  
 298 sputtered Ti neutral atoms in high power impulse magnetron sputtering without reactive gas.  
 299 The scope of this section is to go further on the HiPIMS process studies by investigating the  
 300 Ti atoms AVDF in Reactive(Ar/N<sub>2</sub>)-HiPIMS process (R-HiPIMS), at  $p=2.7$  Pa while the  
 301 discharge power is kept at  $350 \text{ W.cm}^{-2}$ .



302  
 303 **Figure 7:** TR-TDLIF measurements of Ti neutral atoms velocity distribution functions for  
 304 various Ar/N<sub>2</sub> gas mixtures, at  $p=2.7$  Pa,  $z=1.3$  cm,  $R_0=1.3$  cm and  $P=350 \text{ W.cm}^{-2}$ .

305 It is well known that N<sub>2</sub> and N species (neutrals and ions) react with deposited titanium atoms  
 306 on the substrate forming titanium nitride (TiN), and they also react with the reactor walls and  
 307 the target surface. The latter process is called “poisoning of the target”.

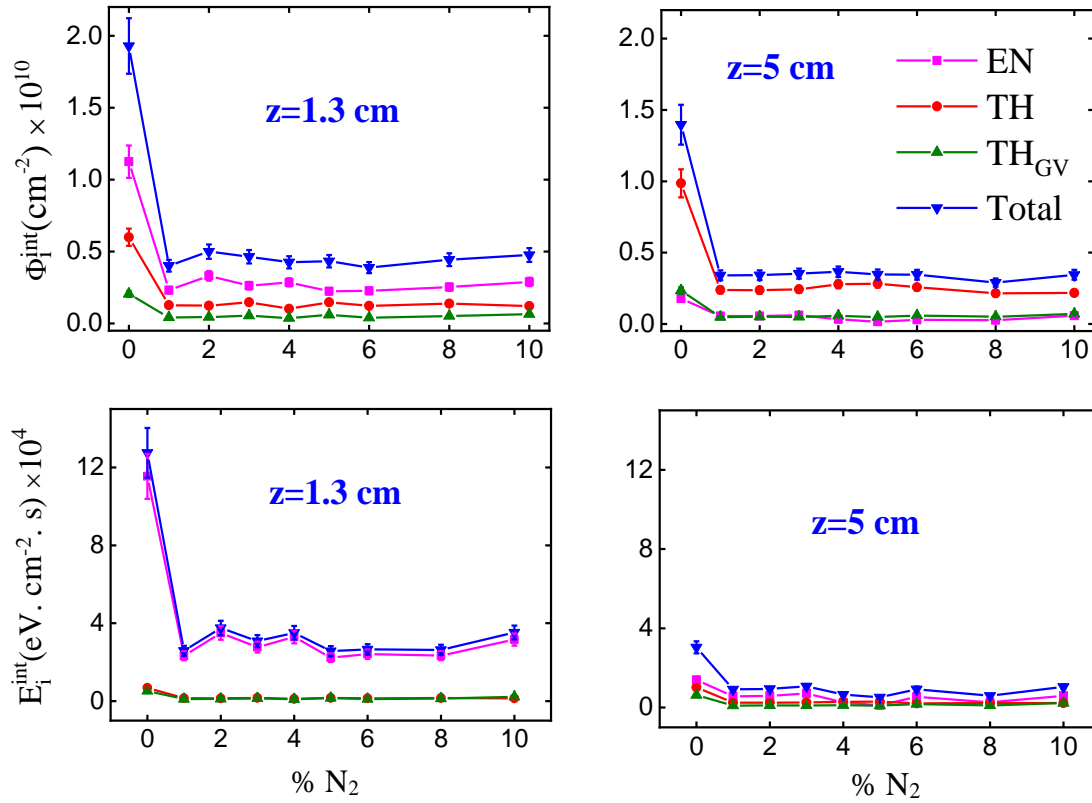


308  
 309 **Figure 8:** Temporal evolutions of deposited flux of energetic (a), quasi-thermalized (b) and  
 310 thermalized (c) atoms as function of Ar/N<sub>2</sub> gas mixture. Time variations of deposited energy of  
 311 energetic (d), quasi-thermalized (e) and thermalized (f) atoms for various Ar/N<sub>2</sub> gas mixtures.  
 312  $P=350W.cm^{-2}$ ,  $z=1.3$  cm,  $R_0=1.3$  cm,  $p=2.7$  Pa.

313 The N<sub>2</sub> addition in the gas mixture (%N<sub>2</sub>) induces changes of all process parameters, among  
 314 them, the cathode voltage ( $U_{cathode}$ ), electron density, yield of secondary electrons emitted  
 315 from the cathode and the Ti sputtering yield. In our conditions ( $0 \leq \%N_2 \leq 10$  % leading to -  
 316  $550 \leq U_{cathode} \leq 450$  V), the yield of secondary electrons is slightly modified with the formation  
 317 of TiN compound layer on the target [44]. In order to evaluate the %N<sub>2</sub> influence on the  
 318 sputtering yield, sputtered titanium neutral atoms AVDFs were measured for various gas  
 319 mixtures near to magnetron target at  $z=1.3$  cm (figure 7). One can see that in pure Ar the  
 320 maximum of the AVDF(t) reaches  $1.4 \times 10^8$  (cm<sup>-4</sup>·s). Adding nitrogen, the distributions show  
 321 that fewer sputtered atoms are detected (the maximum is about  $0.3 \times 10^8$  (cm<sup>-4</sup>·s)) whatever is  
 322 the %N<sub>2</sub>. The poisoning seems to strongly occur on the target and much less Ti atoms are  
 323 sputtered in our conditions. Indeed, the chemical (covalent) Ti-N compound bond strength is  
 324 much stronger than the Ti-Ti metallic one (8.04 eV [45] and 6.6 eV, respectively). Figure 8  
 325 reports time variations of deposited flux and energy of EN, TH and QTH populations  
 326 calculated from results of figure 7. They drastically decrease from %N<sub>2</sub>=1 % and no  
 327 significant changes can be noticed on temporal evolutions up to 10 %.

328 The deposited flux ( $\Phi_i^{int}$ ) and energy ( $E_i^{int}$ ) integrated over a HiPIMS period (using equations  
 329 (5) and (6)) are plotted in figure 9 as a function of %N<sub>2</sub> and for  $z=1.3$ , 3 and 5 cm. It is worth

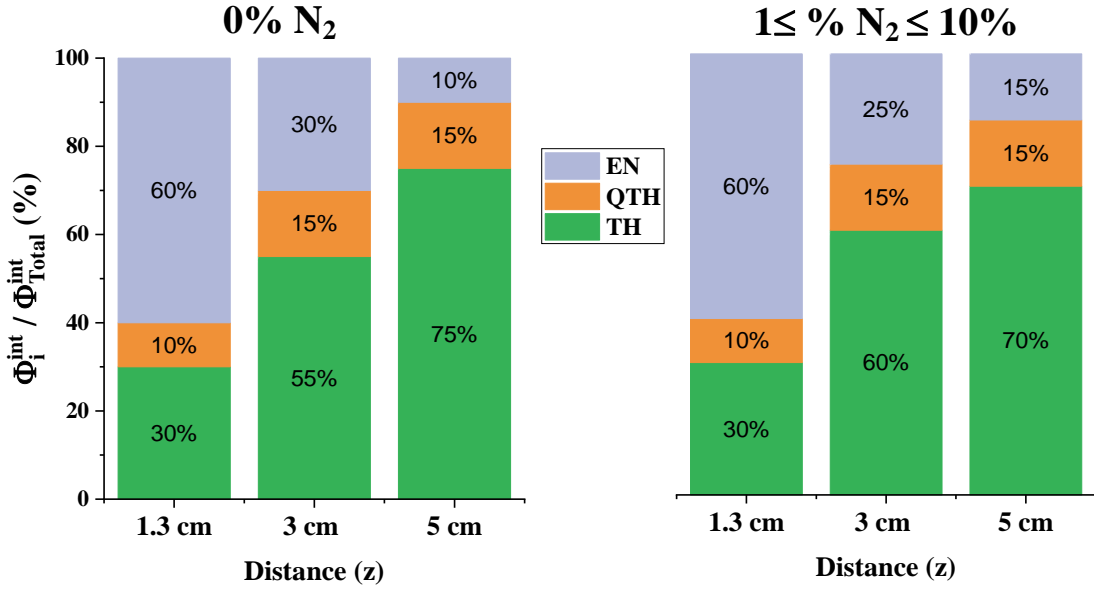
330 noting that  $\Phi_{\text{Total}}^{\text{int}} = \Phi_{\text{EN}}^{\text{int}} + \Phi_{\text{QTH}}^{\text{int}} + \Phi_{\text{TH}}^{\text{int}}$  and  $E_{\text{Total}}^{\text{int}} = E_{\text{EN}}^{\text{int}} + E_{\text{QTH}}^{\text{int}} + E_{\text{TH}}^{\text{int}}$ . According to  
 331 figure 8 ( $z=1.3$  cm), the flux and energy directed toward the substrate (or the probed volume)  
 332 of each population have the same %N<sub>2</sub> dependency behavior up to  $z=5$  cm. This seems to  
 333 confirm that the drastic decrease from %N<sub>2</sub>=1 % is mainly due to poisoning of the target and  
 334 that the transport processes (collisions) of each population are not significantly influenced by  
 335 the amount of nitrogen in the gas mixture (below 10 %). Furthermore, from figure 9, we can  
 336 deduce that, whatever is the %N<sub>2</sub> (see figure 10),  $\Phi_{\text{EN}}^{\text{int}}$  ( $z=1.3$  cm) corresponds to ~60 % of  
 337 the total flux  $\Phi_{\text{Total}}^{\text{int}}$ ,  $\Phi_{\text{TH}}^{\text{int}} \sim 30$  % and  $\Phi_{\text{QTH}}^{\text{int}} \sim 10$  %. At  $z=3$  cm, the proportion of EN flux  
 338 drops to 25-30 %, the TH one becomes the highest (55-60 %) and the QTH one is more  
 339 significant (15 %). Further away from the target ( $z=5$  cm),  $\Phi_{\text{TH}}^{\text{int}}$  is clearly dominant (70-75  
 340 %) but, as mentioned above (description of figure 4),  $E_{\text{EN}}^{\text{int}}$  remains the highest (due to high  
 341  $\langle v \rangle$ ).



342

343 **Figure 9:** Variations of deposited fluxes ( $\Phi_{\text{EN}}^{\text{int}}$ ,  $\Phi_{\text{QTH}}^{\text{int}}$ ,  $\Phi_{\text{TH}}^{\text{int}}$ ,  $\Phi_{\text{Total}}^{\text{int}}$ ) as a function of %N<sub>2</sub> (on the  
 344 left side). Evolutions of corresponding deposited energies ( $E_{\text{EN}}^{\text{int}}$ ,  $E_{\text{QTH}}^{\text{int}}$ ,  $E_{\text{TH}}^{\text{int}}$ ,  $E_{\text{Total}}^{\text{int}}$ ) (on the right  
 345 side).  $z=1.3$  and  $5$  cm,  $P=350\text{W.cm}^{-2}$ ,  $R_0=1.3$  cm,  $p=2.7$  Pa.

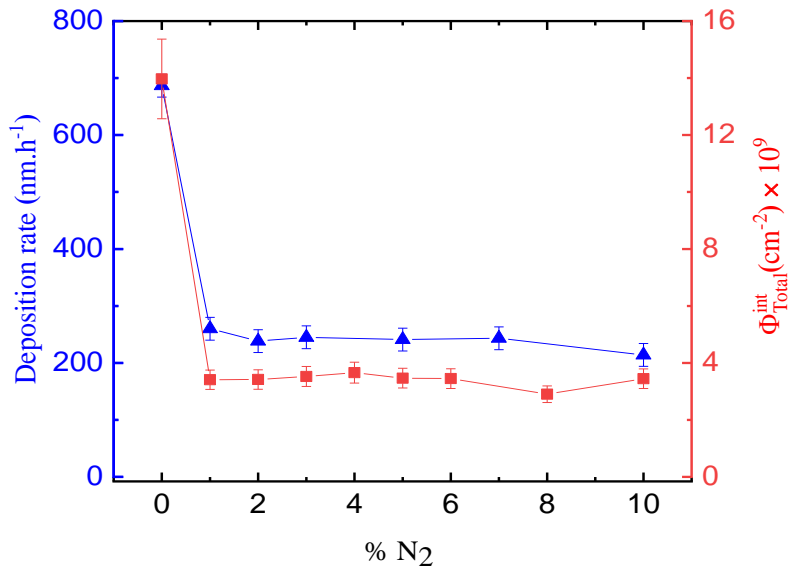
346 These accurate measurements (time and space resolved) of energy and flux of neutral  
 347 deposited species could be used to control and tune the properties of thin films (morphology,  
 348 roughness, crystallinity, density or porosity, etc.) [46-48].



349

350 **Figure 10:** Fraction (%) of the deposited flux of each population ( $\Phi_{EN}^{int}$ ,  $\Phi_{QTH}^{int}$ ,  $\Phi_{TH}^{int}$ ) as a fonction  
 351 of the distance (z), at %N<sub>2</sub>=0% (left side) and 1≤%N<sub>2</sub>≤10 % (right side).

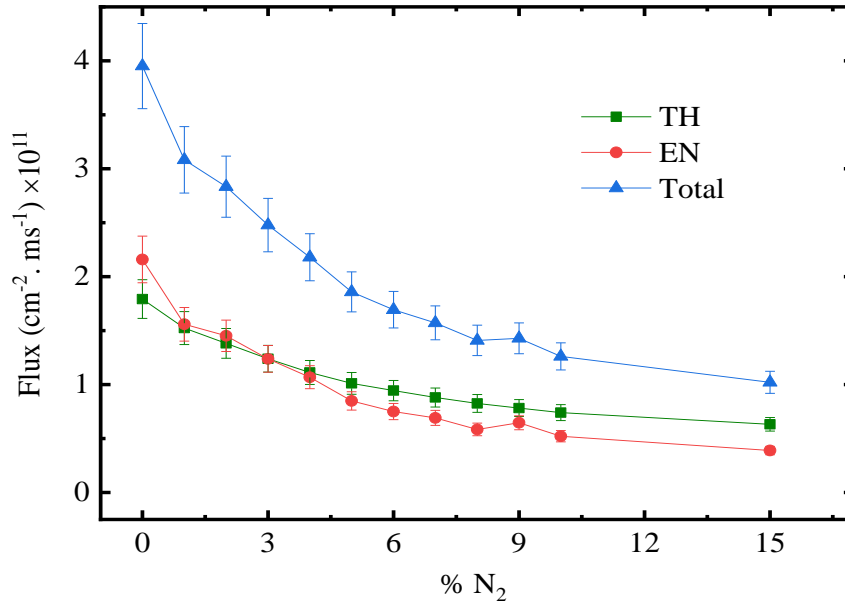
352 In order to verify if our  $\Phi_{Total}^{int}$  measurements of Ti neutral atoms are well representative of all  
 353 deposited species (neutrals and ions), they were compared with the deposition rate measured  
 354 by means of SEM (scanning electron microscopy). Figure 11 shows that  $\Phi_{Total}^{int}$  and the  
 355 deposition rate are in good agreement.



356

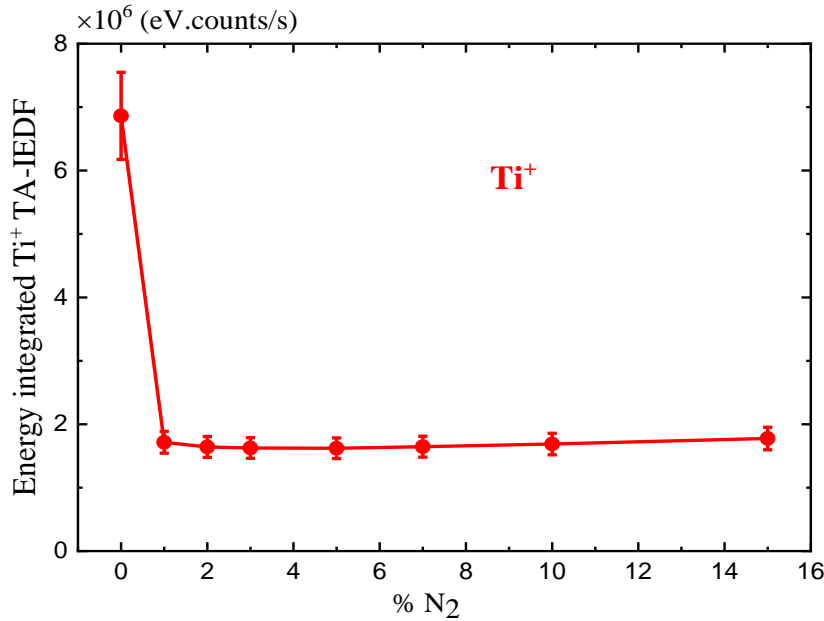
357 **Figure 11:** Variations of the total Ti neutral atoms deposited flux and the deposition rate at z = 5 cm,  
 358 P=350W.cm<sup>-2</sup>, p = 2.7 Pa, R<sub>0</sub>=1.3 cm, as a function of % N<sub>2</sub>.

359 Nevertheless, the influence of %N<sub>2</sub> on deposited flux of Ti neutral atoms in R-HiPIMS  
 360 process was unexpected, *i.e.* we have expected a gradual decrease of  $\Phi_{\text{Total}}^{\text{int}}$  by adding  
 361 nitrogen in gas mixture, as it is usually the case in conventional reactive direct current process  
 362 (figure 12 points out this well-known phenomenon in our R-dcMS conditions)



363  
 364 **Figure 12:** Variations of fluxes of Ti neutral atoms in DC discharge measured with TD-LIF, as a  
 365 function of percentage of N<sub>2</sub>, at  $z=5$  cm,  $p=1.3$  Pa,  $P=5W.cm^{-2}$  and  $R_0=1.3$  cm.  
 366

367 In HiPIMS process, the non-variation of  $\Phi_{\text{Total}}^{\text{int}}$  in the %N<sub>2</sub> range from 1 to 10 % may be  
 368 implied by the gradual decrease of neutral Ti atoms ionization by adding nitrogen molecules  
 369 in the argon gas. Indeed, the degree of ionization of the sputtered atoms may **gradually**  
 370 **decrease with increasing %N<sub>2</sub>**, therefore the number of measured neutral atoms is **higher** than  
 371 expected. To verify this possible assumption, Ti<sup>+</sup> time average ion energy distribution  
 372 functions (TA-IEDF) were determined making use of mass spectrometry (Hiden EQP 300;  
 373 Energy range between 0 and 100 eV). The total Ti<sup>+</sup> deposited flux was calculated integrating  
 374 TA-IEDF with respect to energy (Figure 13). The variations, as a function of %N<sub>2</sub>, of Ti<sup>+</sup> flux  
 375 and  $\Phi_{\text{Total}}^{\text{int}}$  are alike. These very similar evolutions seem to prove that this unexpected  
 376 behavior initially observed on  $\Phi_{\text{Total}}^{\text{int}}$  cannot be explained by Ti ionization degree  
 377 modification but is mainly due to the strong poisoning of the target from %N<sub>2</sub>=1 %. We  
 378 assume that in our HiPIMS conditions (at %N<sub>2</sub>=1 %), the poisoning occurs during the  
 379 relatively long post-discharge (1 ms) and the chosen short discharge time (10 μs), the latter is  
 380 not enough to remove the compound layer from the target in such a way as to be able to  
 381 increase the poisoning process with %N<sub>2</sub>>1 %. In R-dcMS process, the sputtering occurring  
 382 continuously, the poisoning of the target is amplified with %N<sub>2</sub>. **Furthermore, this behavior**  
 383 **and the fact that the deposition rate is governed by the contribution of the neutrals may be**  
 384 **probably due to the small power during the short HiPIMS pulse (small ionization degree of Ti**  
 385 **atoms).**



386

387 **Figure 13:** Variations of energy integrated  $Ti^+$  TA-IEDF (time average-ion energy distribution  
 388 function) obtained by mass spectrometry, at  $z = 5$  cm,  $p = 2.7$  Pa,  $P=350$  W.cm<sup>-2</sup>,  $R_0 = 1.3$  cm, as a  
 389 function of %N<sub>2</sub>.

## 390 IV. Conclusion

391

392 This work was mainly focused on the characterization of sputtered titanium neutral atoms  
 393 transport in reactive (Ar/N<sub>2</sub> gas mixture) HiPIMS process. Time resolved tunable diode laser  
 394 induced fluorescence (TR-TDLIF) measurements, originally developed to study the transport  
 395 of tungsten atoms in non-reactive HiPIMS process [39], were performed to determine Ti  
 396 atoms velocity distribution function (AVDF). From the analysis of the AVDF, three  
 397 populations were detected and studied, *i.e.* the energetic (EN) sputtered atoms population  
 398 (ballistic regime of transport), the thermalized (TH) atoms one (diffusive transport) and a  
 399 third one was highlighted (named “QTH: Quasi Thermalized Atoms”). The latter corresponds  
 400 to EN sputtered atoms which have undergone up to 5-6 collisions with the buffer gas, while 7-  
 401 8 collisions are needed to reach a complete isotropic (axial mean velocity=zero) velocity  
 402 distribution function. This means that this population of QTH atoms has a regime of transport  
 403 close to the TH one but with an axial mean velocity directed towards the probed volume (or  
 404 the substrate). Spatial studies, as a function of the distance from the target, indicate that the  
 405 drop of EN atoms flux is mainly due to dispersion in the sputtering emission cone. The real  
 406 effect of collisions on EN atoms losses is not clearly observed below 5 cm from the target,  
 407 even at 2.7 Pa. Furthermore, it was shown that the transport processes (collisions with the  
 408 buffer gas and Ti ionization degree), and consequently the flux fraction, of each population  
 409 are not significantly influenced by the proportion of nitrogen in the gas mixture (up to 10 %).  
 410 A direct comparison with the deposition rate allowed the consideration of the measurements  
 411 on Ti neutral atoms as being well representative of the total deposited atoms (neutrals and  
 412 ions). Thus, this direct characterization of deposited atoms properties being accessible at  
 413 distance typically used in the industry (5-10 cm from the target), TR-TDLIF measurements of

414 deposited flux and energy can be exploited to tune thin film physical properties. Also such  
415 space-time experimental data may be useful for R-HiPIMS process modelling (as input data  
416 or benchmarks).

## 417 **References**

418

419 [1] Thornton, J. A. (1978). *Journal of Vacuum Science and Technology*, 15(2), 171-177.

420 [2] Mahieu, S., Ghekiere, P., De Winter, G., Heirwegh, S., Depla, D., De Gryse, R. & Van  
421 Tendeloo, G. (2005). *Journal of crystal growth*, 279(1-2), 100-109.

422 [3] Powell, R. A. & Rossnagel, S. (1999). *PVD for Microelectronics: Sputter Deposition*  
423 *Applied to Semiconductor Manufacturing (Thin Films) Academic Press, London.*

424 [4] Rossnagel, S. M., & Hopwood, J. (1994). *Journal of Vacuum Science & Technology B:*  
425 *Microelectronics and Nanometer Structures Processing, Measurement, and Phenomena,*  
426 *12(1), 449-453.*

427 [5] Zhong, G., & Hopwood, J. (1999). *Journal of Vacuum Science & Technology B:*  
428 *Microelectronics and Nanometer Structures Processing, Measurement, and Phenomena,*  
429 *17(2), 405-409.*

430 [6] Rossnagel, S. M. (1998). *Journal of Vacuum Science & Technology B: Microelectronics*  
431 *and Nanometer Structures Processing, Measurement, and Phenomena*, 16(5), 2585-2608.

432 [7] Hopwood, J. (1998). *Physics of Plasmas*, 5(5), 1624-1631.

433 [8] Bretagne, J., Laporte, C. B., Gousset, G., Leroy, O., Minea, T. M., Pagnon, D., ... &  
434 Touzeau, M. (2003). *Plasma Sources Science and Technology*, 12(4), S33.

435 [9] Zhang, J. Q., Setsuhara, Y., Ariyasu, T., & Miyake, S. (1996). *Journal of Vacuum Science*  
436 *& Technology A: Vacuum, Surfaces, and Films*, 14(4), 2163-2168.

437 [10] Yonesu, A., Kato, T., Takemoto, H., Nishimura, N., & Yamashiro, Y. (1999). *Japanese*  
438 *journal of applied physics*, 38(7S), 4326.

439 [11] Boisse-Laporte, C., Leroy, O., De Poucques, L., Agius, B., Bretagne, J., Hugon, M. C., ...  
440 & Touzeau, M. (2004). *Surface and Coatings Technology*, 179(2-3), 176-181.

441 [12] Nouvellon, C., Konstantinidis, S., Dauchot, J. P., Wautelet, M., Jouan, P. Y., Ricard, A.,  
442 & Hecq, M. (2002). *Journal of applied physics*, 92(1), 32-36.

443 [13] Yamashita, M., Setsuhara, Y., Miyake, S., Kumagai, M., Shoji, T., & Musil, J. (1999).  
444 *Japanese journal of applied physics*, 38(7S), 4291.

- 445 [14] Foster, J. E., Wang, W., Wendt, A. E., & Booske, J. (1998). *Journal of Vacuum Science*  
446 *& Technology B: Microelectronics and Nanometer Structures Processing, Measurement, and*  
447 *Phenomena*, 16(2), 532-535.
- 448 [15] Imbert, J. C., De Pouques, L., Boisse-Laporte, C., Bretagne, J., Hugon, M. C., Pagnon,  
449 D., ... & Touzeau, M. (2008). *Thin Solid Films*, 516(15), 4700-4708.
- 450 [16] Kouznetsov, V., Macak, K., Schneider, J. M., Helmersson, U., & Petrov, I. (1999).  
451 *Surface and coatings technology*, 122(2-3), 290-293.
- 452 [17] Anders, A. (2014). *Surface and Coatings Technology*, 257, 308-325.
- 453 [18] Gudmundsson, J. T., Alami, J., & Helmersson, U. (2002). *Surface and Coatings*  
454 *Technology*, 161(2-3), 249-256.
- 455 [19] Bugaev, S. P., Podkovyrov, V. G., Oskomov, K. V., Smaykina, S. V., & Sochugov, N.  
456 S. (2001). *Thin Solid Films*, 389(1-2), 16-26.
- 457 [20] Christie, D. J. (2005). *Journal of Vacuum Science & Technology A: Vacuum, Surfaces,*  
458 *and Films*, 23(2), 330-335.
- 459 [21] Vlček, J., Pajdarová, A. D., & Musil, J. (2004). *Contributions to Plasma Physics*, 44(5-  
460 6), 426-436.
- 461 [22] Alami, J., Gudmundsson, J. T., Bohlmark, J., Birch, J., & Helmersson, U. (2005). *Plasma*  
462 *Sources Science and Technology*, 14(3), 525.
- 463 [23] Ehiasarian A P, Münz, W.-D. Hultman, L. and Helmersson, U. (April 13-18, 2002, Lake  
464 Buena Vista, Florida). *45th annual Technical Conference Proceedings (Society of Vacuum*  
465 *Coaters)*, 328.
- 466 [24] Lattemann, M., Ehiasarian, A. P., Bohlmark, J., Persson, P. Å. O., & Helmersson, U.  
467 (2006). *Surface and Coatings Technology*, 200(22-23), 6495-6499.
- 468 [25] Macák, K., Kouznetsov, V., Schneider, J., Helmersson, U., & Petrov, I. (2000). *Journal*  
469 *of Vacuum Science & Technology A: Vacuum, Surfaces, and Films*, 18(4), 1533-1537.
- 470 [26] Anders, A. (2017). *Journal of Applied Physics*, 121(17), 171101.
- 471 [27] Aiempnanakit, M., Helmersson, U., Aijaz, A., Larsson, P., Magnusson, R., Jensen, J., &  
472 Kubart, T. (2011). *Surface and Coatings Technology*, 205(20), 4828-4831.
- 473 [28] Ferrec, A., Kéraudy, J., & Jouan, P. Y. (2016). *Applied Surface Science*, 390, 497-505.
- 474 [29] Ehiasarian, A. P., Vetushka, A., Hecimovic, A., & Konstantinidis, S. (2008). *Journal of*  
475 *Applied Physics*, 104(8), 083305.

- 476 [30] Palmucci, M., Britun, N., Silva, T., Snyders, R., & Konstantinidis, S. (2013). *Journal of*  
477 *Physics D: Applied Physics*, 46(21), 215201.
- 478 [31] Greczynski, G., & Hultman, L. (2010). *Vacuum*, 84(9), 1159-1170.
- 479 [32] Franz, R., Clavero, C., Kolbeck, J., & Anders, A. (2016). *Plasma Sources Science and*  
480 *Technology*, 25(1), 015022.
- 481 [33] Britun, N., Minea, T., Konstantinidis, S., & Snyders, R. (2014). *Journal of Physics D:*  
482 *Applied Physics*, 47(22), 224001.
- 483 [34] Vasina, P., Fekete, M., Hnilica, J., Klein, P., Dosoudilová, L., Dvorák, P., & Navrátil, Z.  
484 (2015). *Plasma Sources Science Technology*, 24(6).
- 485 [35] Palmucci, M., Britun, N., Konstantinidis, S., & Snyders, R. (2013). *Journal of applied*  
486 *physics*, 114(11), 113302.
- 487 [36] de Poucques, L., Imbert, J. C., Boisse-Laporte, C., Bretagne, J., Ganciu, M., Teulé-Gay,  
488 L., & Touzeau, M. (2006). *Plasma Sources Science and Technology*, 15(4), 661.
- 489 [37] Held, J., Hecimovic, A., von Keudell, A., & Schulz-von der Gathen, V. (2018). *Plasma*  
490 *Sources Science and Technology*, 27(10), 105012.
- 491 [38] Desecures, M., de Poucques, L., Easwarakhanthan, T., & Bougdira, J. (2014). *Applied*  
492 *Physics Letters*, 105(18), 181120.
- 493 [39] Desecures, M., de Poucques, L., & Bougdira, J. (2017). *Plasma Sources Science and*  
494 *Technology*, 26(2), 025003.
- 495 [40] Desecures, M., de Poucques, L., & Bougdira, J. (2015). *Plasma Sources Science and*  
496 *Technology*, 24(1), 015012.
- 497 [41] Magnus, F., Sveinsson, O. B., Olafsson, S. & Gudmundsson, J. T.  
498 (2011). *Journal of Applied Physics*, 110(8), 083306.
- 499 [42] Konstantinidis, S., Dauchot, J. P., Ganciu, M., Ricard, A., & Hecq, M. (2006). *Journal of*  
500 *applied physics*, 99(1), 013307.
- 501 [43] Sushkov, V., Do, H. T., Cada, M., Hubicka, Z., & Hippler, R. (2013). *Plasma Sources*  
502 *Science and Technology*, 22, 015002.
- 503 [44] Depla, D., Mahieu, S., & De Gryse, R. (2009). *Thin Solid Films*, 517(9), 2825-2839.
- 504 [45] Du, L., Edgar, J. H., Kenik, E. A., & Meyer, H. (2010). *Journal of Materials Science:*  
505 *Materials in Electronics*, 21(1), 78.
- 506 [46] Sarakinos K, Alami J and Konstantinidis S 2010. *Surf. Coat. Technol.* 204 1661–84.

- 507 [47] Samuelsson M, Lundin D, Jensen J, Raadu M A, Gudmundsson J T and Helmersson U  
508 (2010). *Surf. Coat. Technol.* 205 591–6.
- 509 [48] Kersten H, Deutsch H, Steffen H, Kroesen G M W and Hippler R (2001) *Vacuum* 63  
510 385–431.